Aspects of Delay-Doppler Filtering in OFDM Passive Radar

Stephen Searle
University of South Australia

Daniel Gustainis, Brendan Hennessy, Robert Young
Defence Science and Technology Group, Australia

***Abstract*—Delay-Doppler filtering enables the isolation of radar returns from a designated region of the ambiguity plane. Such returns can be cancelled from the surveillance signal, lowering the ambiguity floor and reducing demands on dynamic range. Modern passive radar systems frequently use OFDM-based illuminators of opportunity, and recent studies have demonstrated how the structure of OFDM signals can be exploited to perform delay-Doppler filtering in the frequency domain. In this study several aspects of one such algorithm are investigated: the ability to cancel returns when delay is not a whole number of samples; the ability to conserve computation by approximating a projection matrix; the effect of returns having delays exceeding the OFDM guard interval; and the application of the method to extended targets. The consideration of these aspects demonstrates the efficacy of the method in situations common to passive radar.**

I. Introduction

Many modern communication signals employ Orthogonal Frequency Division Multiplexing (OFDM) modulation. Such signals are typically of large bandwidth and have favourable autocorrelation properties. The prevalence and properties of OFDM signals makes them ideal Illuminators Of Opportunity (IOOs) for Passive Bistatic Radar (PBR) [1]. Recent research in the field of passive radar has exploited many diverse OFDM-modulated signals, including DAB [2], DVB-T [3], LTE [4], WiFi [5], and DRM [6].

An ongoing problem in PBR is the presence of Direct Path Interference (DPI) and other Zero Doppler Clutter (ZDC) in the surveillance signal. These unwanted returns are typically of high power despite attempts to suppress them [1], [6]. Their presence increases dynamic range requirements on the receiver, and they can mask the presence of weak targets in the signal. Any DPI and ZDC in the digitised signal is often handled by cancellation [7]. A Wiener filter provides optimal cancellation but is computationally unwieldy. In practice numerical approximations to the Wiener filter or adaptive filters are used [8], [9].

Each sequential OFDM symbol is extended by prepending it with redundant data, the Cyclic Prefix (CP). This is done in order to mitigate the effects of multipath, as it causes the mutual orthogonality of the OFDM subcarriers to be preserved when filtered with a time-delayed copy of the signal. This feature has proven to be beneficial for PBR, as it allows the orthogonality of subcarriers to be exploited in ambiguity computations, resulting in delay-Doppler surfaces with extremely low pedestals [10], [11].

Recently emerging studies have exploited the OFDM CP for purposes of clutter modelling and cancellation. Noting that in the frequency domain a time shift would manifest as a frequency-dependent scalar phasor on each carrier, the ZDC is estimated by projecting the observed time-history of Fourier coefficients at each carrier onto the recovered symbols [6]. Further noting that in the presence of small Doppler shift the scalar phasor would advance over time, the method was adapted to successfully estimate clutter exhibiting small movements [12]. These methods could broadly be described as Doppler filters, selecting and cancelling all returns having near-zero Doppler shift. In response to a need to isolate high-power returns of limited extent and nonzero Doppler shift, the method was further extended to operate on any arbitrary region of the delay-Doppler plane [13].

The purpose of this study is to revisit the method proposed in [13] and expound upon certain of its aspects. The ability to subsample in delay, not easily obtained with a discrete tap-delay Wiener filter, can be achieved with the present method. An approximation is suggested which can reduce the required amount of computation with minimal cost to performance. The long-delay case is investigated, in which the delay of a target return exceeds the duration of the CP, thereby invalidating an assumption of the present method. Finally we demonstrate the ability of the method to isolate extended target returns.

II. Review of ECA+ method

The evolution of Extensive Cancellation Algorithms (ECA) culminating in the ECA+ method for cancellation of arbitrary regions of delay-Doppler in OFDM signals is described in [13] and its references. This section summarises the ECA+ method.

A. Signal Model

An OFDM signal $r(t)$ is formed by the concatenation of OFDM symbols $r_1(t),\ r_2(t),\ r_3(t)\ldots$

$$r(t) = \sum_{j=1}^{J} r_j(t-(j-1)T_e) \tag{1}$$

An OFDM symbol is comprised of K carriers, orthogonal over the duration T_u, each modulated by a datum c_{kj} drawn from a constellation.

$$r_j(t) = \sum_{k=0}^{K-1} c_{kj} e^{i\frac{2\pi}{N_u} f_s k(t-T_g)}\, \Pi(\tfrac{t}{T_e} - \tfrac{1}{2}) \tag{2}$$

The full symbol duration is $T_e = T_u + T_g$ where T_g is the CP duration. $\Pi(\cdot)$ is the rect function with support $(-\frac{1}{2}, \frac{1}{2})$. The useful portion (post-CP) of the jth symbol period begins at time u_j,

$$u_j = (j-1)T_e + T_g \tag{3}$$

and thus the nth useful sample of the jth symbol is

$$r_j[n] = r(u_j + nT_s), \qquad n = 0, 1, \ldots N_u - 1 \tag{4}$$

Consider $x(t)$, a copy of $r(t)$ weighted by a, delayed by τ seconds and Doppler shifted by ν Hz,

$$x(t) = ar(t-\tau)e^{i2\pi\nu t} \tag{5}$$

Note that with short delays ($\tau < T_e$), the pth symbol period of $x(t)$ will contain elements of two consecutive transmitted symbols, $r_p(t)$ and $r_{p-1}(t)$. The samples taken from $x(t)$ in the useful portion of the pth symbol period are

$$x_p[n] = x(u_p + nT_s) \tag{6}$$

$$= ae^{i2\pi\nu(u_p+nT_s)} \sum_{j=1}^{J}\sum_{k=0}^{K-1} c_{kj}e^{i\frac{2\pi}{N_u}f_s k((p-j)T_e+nT_s-\tau)} \times \Pi(\tfrac{(p-j)T_e+nT_s-\tau+T_g}{T_e} - \tfrac{1}{2}) \tag{7}$$

The Discrete Fourier Transform (DFT) of this is

$$X_p[\ell] = \sum_{n=0}^{N_u-1} x_p[n]e^{-i\frac{2\pi}{N_u}\ell n} \tag{8}$$

$$= a\sum_{j=1}^{J}\sum_{k=0}^{K-1} c_{kj}e^{i\frac{2\pi}{N_u}f_s k((p-j)T_e-\tau+N_u u_p\nu)}\rho \tag{9}$$

where

$$\rho = \sum_{n=0}^{N_u-1} \Pi(\tfrac{(p-j)T_e+nT_s-\tau+T_g}{T_e} - \tfrac{1}{2})e^{i\frac{2\pi}{N_u}((k-\ell)n+T_u\nu n)} \tag{10}$$

In the event that $\tau < T_g$ there will be no Inter-Symbol Interference (ISI); that is, only contributions from symbol j will be present in the pth period's DFT. In this case $\Pi(\cdot)$ evaluates to 1 and, providing that $\frac{T_u}{N_u} \ll \nu$, we have $\rho \approx N_u$ for $k = \ell$ and 0 otherwise. The DFT then simplifies to

$$X_p[k] = N_u a c_{pk} e^{-i\frac{2\pi}{N_u}f_s k\tau} e^{i\frac{2\pi}{N_u}N_u u_p\nu} \tag{11}$$

Given a signal comprising M returns, each with parameters $\tilde{a}_m$, τ_m and ν_m, and $\tau_m < T_g\ \forall m$, then the Fourier bin history of the signal over time can be written

$$\mathbf{S} = \mathbf{C} \odot \mathbf{D}\mathbf{A}\mathbf{V}^T \tag{12}$$

where

$$S_{kj} = X_j[k] \tag{13}$$

$$C_{kj} = c_{kj} \tag{14}$$

$$D_{km} = e^{-i\frac{2\pi}{N_u}f_s k\tau_m} \tag{15}$$

$$V_{jm} = e^{i2\pi\nu_m(p-1)T_e} \tag{16}$$

$$\mathbf{A} = \mathrm{diag}(\tilde{a}_1, \ldots, \tilde{a}_M) \tag{17}$$

The columns of $\mathbf{V}$ are the phase-histories over the J symbol periods due to Doppler shift for each of the M components in the signal. Similarly the columns of $\mathbf{D}$ are the phase-responses of the K carriers for the delays of each of the M components.

B. ECA+ Method

Delay in a returned signal weights each OFDM subcarrier by a phase which increases linearly with frequency, and Doppler shift weights each OFDM symbol by a phase which increases with time. The ECA+ method [13] forms clutter subspaces in the frequency domain from phasors corresponding to delays and Doppler shifts of interest. The surveillance signal is projected into these subspaces to estimate the clutter which is then cancelled.

It is assumed that the modulation symbols $\mathbf{C}$ are known, or can be estimated perfectly from a reference signal. This data is removed from the surveillance signal in the frequency domain to produce $\mathbf{Z}$ which is the effects of delay and Doppler shift on the components:

$$Z_{kj} = S_{kj}/c_{kj} \tag{18}$$

Denote Doppler frequencies of interest as $\eta_1, \ldots, \eta_L$, distinct from the frequencies $\nu_1, \ldots, \nu_M$ actually in the signal. The corresponding phase-history vectors can be generated via (16, setting $\nu = \eta_i$), forming a Doppler subspace matrix $\mathbf{Q}$. From this a projection matrix $\mathbf{P_Q}$ can be formed. The data-free signal is filtered in the frequency domain by multiplication with $\mathbf{P_Q}$, preserving components which correlate with the Doppler vectors,

$$Q_{j\ell} = e^{i2\pi\eta_\ell T_e(j-1)} \tag{19}$$

$$\mathbf{P_Q} = \mathbf{Q}(\mathbf{Q}^H\mathbf{Q})^{-1}\mathbf{Q}^H \tag{20}$$

$$\mathbf{Y_Q} = \mathbf{Z}\mathbf{P_Q} \tag{21}$$

Similarly, for a set of delays of interest, corresponding phase-history vectors can be generated via (15) to form a delay subspace matrix $\mathbf{W}$. A projection matrix $\mathbf{P_W}$ formed from this is used to filter the data-free signal, preserving components which correlate with the delay vectors.

$$W_{k\ell} = e^{-i\frac{2\pi}{N_u}f_s k d_\ell} \tag{22}$$

$$\mathbf{P_W} = \mathbf{W}(\mathbf{W}^H\mathbf{W})^{-1}\mathbf{W}^H \tag{23}$$

$$\mathbf{Y_W} = \mathbf{P_W}\mathbf{Z} \tag{24}$$

One can multiply $\mathbf{Z}$ by both $\mathbf{P_W}$ and $\mathbf{P_Q}$ to project the signal into a specific region of delay and Doppler.

$$\mathbf{Y} = \mathbf{P_W}\mathbf{Z}\mathbf{P_Q} \tag{25}$$

The filtered signal can be reconstructed from $\mathbf{Y}$, or the filtered component can be cancelled from the signal by reconstruction with $\mathbf{Z} - \mathbf{Y}$:

$$\mathbf{S}_{\text{filtered}} = \mathbf{Y} \odot \mathbf{C} \tag{26}$$

$$\mathbf{S}_{\text{cancelled}} = (\mathbf{Z} - \mathbf{Y}) \odot \mathbf{C} \tag{27}$$

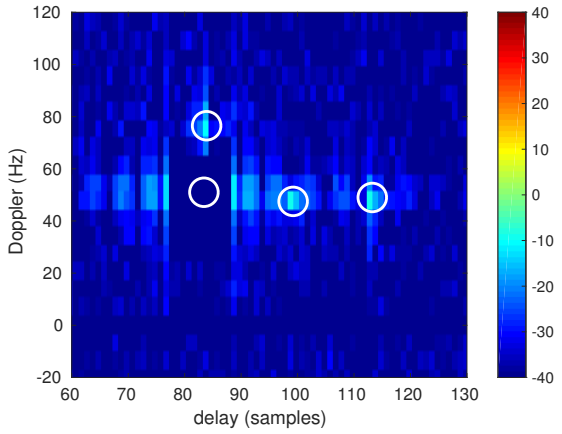

Fig. 1. Delay-Doppler output, Wiener method used to cancel neighbourhood about strong return. Target positions highlighted with circles.

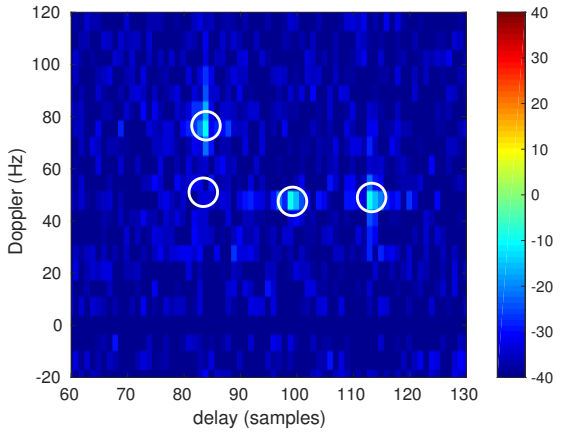

Fig. 2. Delay-Doppler output, ECA+ method with finely-discretised delay basis used to cancel neighbourhood about strong return.

III. Aspects of ECA+ Processing

A. returns having delay of non-integer samples

The Wiener filter interference canceller used as a benchmark in [8], [13] models interference as the output of a tap-delay line filter, the coefficients of which are chosen to minimise the power in the error signal $e[n]$,

$$e[n] = s[n] - \sum_{\ell=0}^{L=1} h[\ell] r[n-\ell] \tag{28}$$

This works well for delays which are a whole number of samples. However returns which sit at delays in between sample points manifest distributed across delay bins in a sinc-like fashion. This is analogous to the response of a discrete Fourier transform to a sinusoid not of centre-bin frequency. Applying a tap-delay canceller will remove power from the specified delays, leaving power outside of these delay bins untouched. The Wiener filter could be reformulated to operate at fractional samples but only at the cost of increased complexity.

The ECA+ method treats delay as a continuous valued quantity. An arbitrary set of delays, which may be discretised more finely than the sample period, can be specified for cancellation. The inclusion of subsample delays in the clutter basis results in removal of contributions which leak outside of the delay region.

Some simulated data, including one strong return and a number of weak returns, was processed with a Wiener filter method. The clutter region was defined at 11 consecutive delay bins (and several Doppler bins) surrounding the strong return. This result first appeared in [13] and is reproduced in figure 1. Power in the defined clutter region has been suppressed by 71 dB but residual power remains outside the delay region. The data was reprocessed with the ECA+ method, defining the clutter region to cover the same delays, but discretised at every half-sample. The result is displayed in figure 2. Power in the clutter region has been suppressed by only 55 dB but there is no residual power outside the delay region.

B. approximation of projection matrix

The delay subspace matrix $\mathbf{W}$ has column dimension N_W being the number of delay points being filtered, and row dimension K being the number of occupied carriers of the OFDM signal. Typically $N_W \ll K$ so the subspace matrix has large nullity. It is thus possible to approximate the projection matrix $\mathbf{P}_\mathbf{W}$ by using a subset of the available carriers, $\kappa \subset \{0, \ldots, K-1\}$.

$$\tilde{W}_{k\ell} = W_{\kappa_k,\ell} = e^{-i\frac{2\pi}{N_u} f_s \kappa_k d_\ell} \tag{29}$$

$$\tilde{Z}_{kj} = Z_{\kappa_k j} \tag{30}$$

$$\tilde{\mathbf{P}}_\mathbf{W} = \mathbf{W}(\tilde{\mathbf{W}}^H \tilde{\mathbf{W}})^{-1} \tilde{\mathbf{W}}^H \tag{31}$$

Note that the leftmost matrix in (31) is the full subspace matrix defined by (22), so the trimmed-carrier data $\tilde{\mathbf{Z}}$ is projected back into the full K carriers. The approximate projection matrix $\tilde{\mathbf{P}}_\mathbf{W}$ may be used in place of $\mathbf{P}_\mathbf{W}$ in equations (24–27).

The cost of evaluating (23) directly involves $LK(2L+K)$ complex multiplications. Employing only $|\kappa|$ of the K carriers can result in considerable savings of computation. A similar approximation could be performed on the Doppler component of the filter, using only a fraction of the timeblocks, but since the number of available timeblocks L is typically an order of magnitude smaller than the number of carriers K the savings will not be as great and we do not explore this here.

A 2-frame OFDM reference signal was simulated, and also a surveillance signal containing returns from two point targets, the stronger being 34 dB above the weaker, and also some additive Gaussian noise. No zero-Doppler clutter was simulated for this example. A delay-Doppler neighbourhood about the strong target was defined, comprising 23 delays spaced at one-half sample. In each of 200 realisations the specified delay-Doppler region was excised using the ECA+ method. The simulation was repeated using a subsets of the available carriers, each subset being different in number but spaced evenly across the available bandwidth. Different levels of Gaussian noise were also considered.

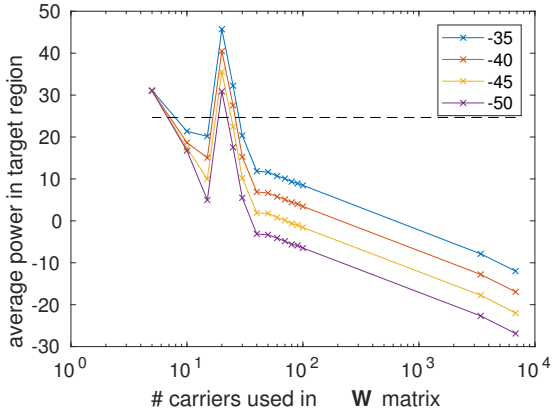

Fig. 3. Average power in the delay-Doppler region of the strong return after its cancellation from the signal, SNR from -35 to -50 dB

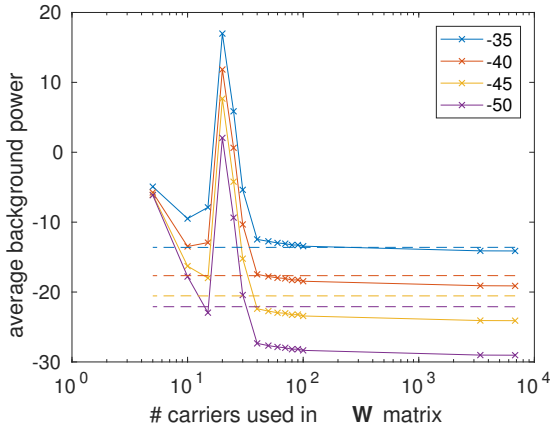

Fig. 4. Average background power in the ambiguity surface after cancellation of the strong return from the signal, SNR from -35 to -50 dB

The average power in a region of delay-Doppler about the strong target's location was computed from the simulation results, and is displayed in figure 3. As the number of carriers used in $\mathbf{W}$ decreases, the amount of power remaining in the cancelled signal also increases until the number of carriers approaches 23, the number of delays being cancelled.

The average level of the ambiguity background is computed from the simulation results and presented in figure 4. At all SNRs the background power is relatively constant for large carrier subsets, increasing only marginally as the number of carriers approaches the number of ranges being cancelled. However this behaviour changes rapidly as $|\kappa| < 40$. The threshold at which the average background power becomes higher than the baseline case (no cancellation) increases as a function of noise power. At low noise power (-50 dB) there is a greater gap between the pedestal due to large return and the noise floor, so that cancellation drops the background by 7 dB when $|\kappa| = K$. This background level is lower than the baseline case provided that $|\kappa| > 32$. However at higher noise (-30 dB) the noise floor contribution is comparable to that of the strong return. Suppressing the strong return only affords an improvement of one half of a dB, which disappears when $|\kappa| < 245$.

If a limit can be placed on performance loss, then for a given delay neighbourhood and noise level a minimum number of carriers can be determined which achieves this limit, saving computation. For the present scenario, choosing a subset of 70 carriers would limit the rise in ambiguity floor to one dB at all noise levels, but would employ .05 of 1 percent of the multiplications required by using all carriers.

C. *delays* $> N_g$

Previous studies employing frequency domain methods [6], [12], [13] have implicitly assumed that no returns in the signal will exhibit a delay greater than the OFDM guard interval N_g, so that the simple expression for DFT (11) always holds. A consequence is that the data recovered from a Fourier bin is equal to the data transmitted on the corresponding carrier, multiplied by a complex constant which is a function of the parameters of the return components. This fact enables the carrier-based delay-Doppler filtering methods.

In the event that one or more returns exhibit a delay exceeding N_g, data from preceding symbols is present in each processing block, causing ISI and affecting the orthogonality of the carriers. The simple expression of (11) will degrade as a function of the delays.

Signals were simulated for a scenario involving one strong target and a number of weaker returns and noise (-40 to -50 dB). The delay of the strong return was varied from 128 to 4096 samples (equivalent to 4.8 to 153 km bistatic range). The guard interval of the OFDM signal N_g was 512 samples. For each delay 100 simulations were performed, in which the strong target was cancelled from the signal via the ECA+ method. The ambiguity surface was generated and the average power in a neighbourhood about the target was computed and averaged over the simulations. Results are presented in figure 5. It can be seen that cancellation is excellent when the delay of the target is less than N_g. However this worsens markedly as the delay increases past N_g.

The simulation was repeated, this time with the strong return at very short delay (10 samples) and varying the delay of a weaker return (-48 dB). This is representative of a realistic scenario where returns from close clutter are expected to be some orders of magnitude larger than those from a distant target. The average power observed at the weak target location was computed, with and without first cancelling the strong return with ECA+. Observations are presented in figure 6. At delays $< N_g$ the power at the weak target location was negligibly smaller when the strong return was cancelled. However at delays above N_g power dropped by up to 0.7 dB, stabilising at this figure at delays above $2N_g$.

D. *Extended targets*

Certain targets can occupy several range-Doppler cells over a CPI. This might be because the target is genuinely extended in range (*e.g.* a train), or because the target moves with sufficiently high velocity that range migration occurs over the CPI duration. Detection of weaker targets is enhanced

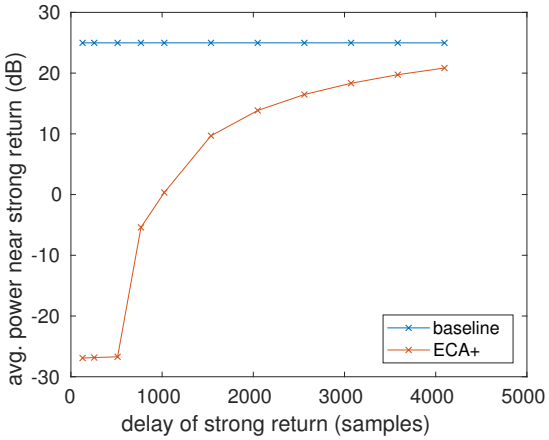

Fig. 5. Average power in neighbourhood of strong return, before (baseline) and after (ECA+) its cancellation, at various delays.

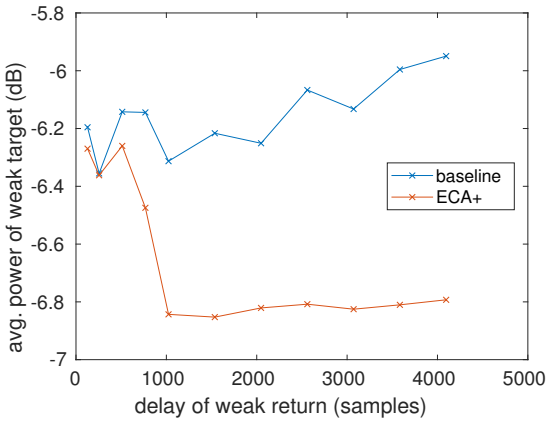

Fig. 6. Average power observed at weak target peak, before (baseline) and after (ECA+) cancellation of strong return

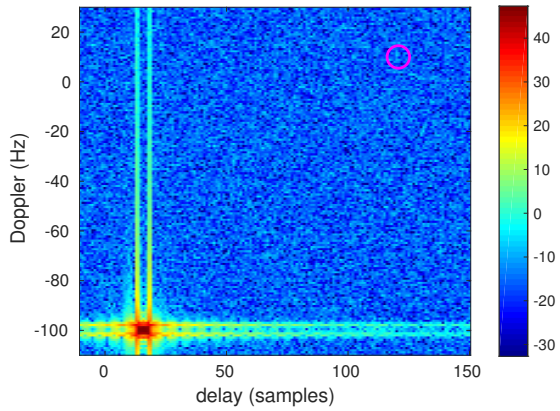

Fig. 7. Cross ambiguity surface, surveillance signal comprising returns from strong fast target, weak slow target and noise.

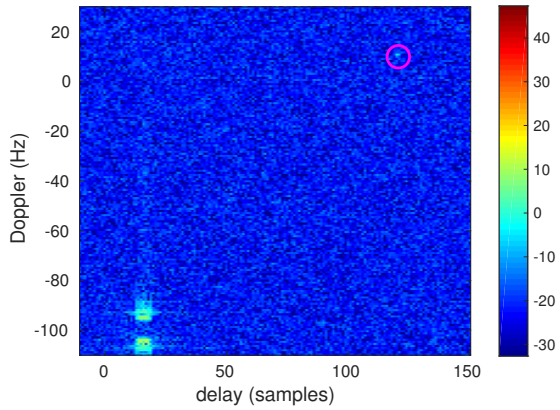

Fig. 8. Cross ambiguity surface, cancelled surveillance signal comprising weak slow target and noise.

by integrating over longer CPIs, which exacerbates the extent of fast-moving targets. Isolation and excision of such targets can be problematic. The target's precise occupancy in delay–Doppler cannot be known, and it will be present in between delay bins and Doppler bins. This renders a tap-delay Wiener filter solution [13] impractical. An ECA-CD algorithm [12] modified to suppress a range of Doppler returns in the vicinity of the target is feasible, but will remove power at all delays in that Doppler region. The ECA+ method is well-suited to isolation of extended targets in OFDM PBR because it permits filtering of an arbitrary neighbourhood of the ambiguity surface, oversampling in both delay and Doppler, without the computational expense of a full Wiener filter.

An 8K-mode 7 MHz DVB-T signal of 16 frames (1.18 s) was generated. A PBR surveillance signal was generated by computing returns of this signal from a fast target (speed 100 m/s) and a slow weaker target (-60 dB with respect to fast return, speed 10 m/s) and combining them. The fast target is expected to transit through several delay bins over the processing interval. Gaussian noise of power -53 dB was added. No direct-path or zero-Doppler clutter returns were added in this example. The cross-ambiguity surface of the DVB-T signal with the surveillance signal was computed and is presented in figure 7. Note the extended region of delay-Doppler occupied by the strong fast target in the lower left region, encompassing several delay bins. After the long CPI the weaker target's power is measured to be 11 dB greater than the floor power. Nevertheless the strong target dominates and it is desirable to remove this. A neighbourhood about the extended target was defined, extending to three Doppler bins either side and discretised to 0.5 of a Doppler bin, and extending to 2 delay bins either side of the target's extent, discretised to 0.5 of a range bin. The neighbourhood is thus not small, comprising 273 delay-Doppler points. The ECA+ algorithm was used to estimate the returns at these delay-Doppler points and cancel them from the signal. The cross-ambiguity was recomputed with the cancelled signal and is presented in figure 8. Removing the strong extended target drops the ambiguity floor by 7 dB in this case, improving target SINR accordingly.

IV. Conclusion

This study has investigated several aspects of the ECA+ method. The benefit over tap-delay filter methods has been

demonstrated by a comparison with a standard Wiener filter interference canceller. The ability to specify continuous-valued delays allows leakage of power from outside the delay region of interest to be cancelled.

Computation can be significantly expedited through approximation of the projection matrix using a subset of available carrier information. The trade-off for performance is a small increase in ambiguity floor; the number of carriers $|\kappa|$ can be chosen to keep this at an acceptable level.

The ECA+ method implicitly assumes that any target delays are shorter than the guard interval; when this is not the case, ISI causes target energy to leak from the OFDM frequency bins. Simulation study has determined that cancellation performance is affected significantly when the designated clutter return has delay exceeding N_g. However in radar typically the strong clutter returns exist at short delays. Simulation results have suggested that the power of weak targets at large delay will be attenuated by a small amount.

The ability of ECA+ to remove extended targets in delay and Doppler has been demonstrated by simulation. This enables passive radar to employ long integration times, as strong returns from targets migrating through several range-Doppler cells can still be excised.

REFERENCES

[1] C. R. Berger, B. Demissie, J. Heckenbach, P. Willett, and S. Zhou, "Signal processing for passive radar using OFDM waveforms," *IEEE Journal of Selected Topics in Signal Processing*, vol. 4, pp. 226–238, Feb 2010.

[2] D. W. O'Hagan, H. Kuschel, J. Heckenbach, M. Ummenhofer, and J. Schell, "Signal reconstruction as an effective means of detecting targets in a DAB-based PBR," in *11th International Radar Symposium*, pp. 1–4, June 2010.

[3] J. E. Palmer, H. A. Harms, S. J. Searle, and L. Davis, "DVB-T passive radar signal processing," *IEEE Transactions on Signal Processing*, vol. 61, pp. 2116–2126, April 2013.

[4] A. Evers and J. A. Jackson, "Analysis of an LTE waveform for radar applications," in *2014 IEEE Radar Conference*, pp. 200–205, May 2014.

[5] F. Colone, P. Falcone, C. Bongioanni, and P. Lombardo, "Wifi-based passive bistatic radar: Data processing schemes and experimental results," *IEEE Transactions on Aerospace and Electronic Systems*, vol. 48, pp. 1061–1079, APRIL 2012.

[6] Z. Zhao, X. Wan, Q. Shao, Z. Gong, and F. Cheng, "Multipath clutter rejection for digital radio mondiale-based HF passive bistatic radar with OFDM waveform," *IET Radar, Sonar Navigation*, vol. 6, pp. 867–872, December 2012.

[7] F. Colone, D. W. O'Hagan, P. Lombardo, and C. J. Baker, "A multistage processing algorithm for disturbance removal and target detection in passive bistatic radar," *IEEE Transactions on Aerospace and Electronic Systems*, vol. 45, pp. 698–722, April 2009.

[8] J. E. Palmer and S. J. Searle, "Evaluation of adaptive filter algorithms for clutter cancellation in passive bistatic radar," in *2012 IEEE Radar Conference*, pp. 0493–0498, May 2012.

[9] J. L. Garry, C. J. Baker, and G. E. Smith, "Evaluation of direct signal suppression for passive radar," *IEEE Transactions on Geoscience and Remote Sensing*, vol. 55, pp. 3786–3799, July 2017.

[10] D. Poullin, "Passive detection using digital broadcasters (DAB, DVB) with COFDM modulation," *IEE Proceedings - Radar, Sonar and Navigation*, vol. 152, pp. 143–152, June 2005.

[11] S. Searle, J. Palmer, L. Davis, D. W. O'Hagan, and M. Ummenhofer, "Evaluation of the ambiguity function for passive radar with OFDM transmissions," in *2014 IEEE Radar Conference*, pp. 1040–1045, May 2014.

[12] C. Schwark and D. Cristallini, "Advanced multipath clutter cancellation in OFDM-based passive radar systems," in *2016 IEEE Radar Conference (RadarConf)*, pp. 1–4, May 2016.

[13] S. Searle, D. Gustainis, B. Hennessy, and R. Young, "Cancelling strong doppler shifted returns in OFDM based passive radar," in *2018 IEEE Radar Conference (RadarConf18)*, pp. 0359–0354, April 2018.